An opinion on the multiscale nature of Covid-19 type disease spread

Swetaprovo Chaudhuri[1], Abhishek Saha[2] and Saptarshi Basu[3]

Abstract

Recognizing the multiscale, interdisciplinary nature of the Covid-19 transmission dynamics, we discuss some recent developments concerning an attempt to construct a disease spread model from the flow physics of infectious droplets and aerosols and the frequency of contact between susceptible individuals with the infectious aerosol cloud. Such an approach begins with the exhalation event−specific, respiratory droplet size distribution (both airborne/aerosolized and ballistic droplets), followed by tracking its evolution in the exhaled air to estimate the probability of infection and the rate constants of the disease spread model. The basic formulations and structure of submodels, experiments involved to validate those submodels, are discussed. Finally, in the context of preventive measures, respiratory droplet−face mask interactions are described.

Addresses

[1]Institute for Aerospace Studies, University of Toronto, Toronto, ON M3H 5T6, Canada
[2]Department of Mechanical and Aerospace Engineering, University of California San Diego, La Jolla, CA 92093, USA
[3]Department of Mechanical Engineering, Indian Institute of Science, Bengaluru, KA 560012, India

Corresponding authors: S. Basu (sbasu@iisc.ac.in); S. Chaudhuri (schaudhuri@utias.utoronto.ca)

Introduction

At the time of writing this article, the cumulative number of Covid-19 (coronavirus disease 2019) positive cases in the world is close to 135 million, with nearly 3 million deaths. However, it has been recognized that the actual number of cases could be far higher than the reported number. Li et al. [1] estimated that in China, "86% of all infections were undocumented [95% credible interval (CI): 82−90%] before the 23 January 2020 travel restrictions." A major impediment in the direct estimation of the total number of actual positive cases in the Covid-19 pandemic has been the vast number of asymptomatic cases [2−5]. Subramanian et al. [5] noted, 'Using a model that incorporates daily testing information fit to the case and serology data from New York City, we show that the proportion of symptomatic cases is low, ranging from 13 to 18%, and that the reproductive number may be larger than often assumed.' However, in many cases, for predictions, epidemiological models utilize the reported/available data to obtain the model (ordinary differential equations [ODEs]) parameters toward estimation of the basic reproduction number. The role and power of present epidemiological models in determining policy and implementation of nonpharmaceutical interventions such as social distancing and lockdown cannot be overemphasized [6−8]. At the same time, the lack of availability of actual infection numbers, possible dependency and sensitivity of the model parameters on seasonality [9−11], and mechanism of disease transfer behoove a physics-based approach wherein the model parameters are derived from first principles calculations. Indeed, such an approach, if possible, is not without limitations and uncertainties and must be reconciled with data for practical implementations. More importantly, such an approach calls for a detailed mechanistic understanding of each of the several subcomponents that span across scientific disciplines and integration of ostensibly decoupled fields such as virus kinetics inside aerosols, droplet evaporation, turbulent diffusion, human mobility, human behavior, their modeling, and the uncertainties thereof. These subcomponents span across multiple length and time scales, as shown in Figure 1, and are not uniformly at the same level of understanding. Yet, given the extremely high stakes a catastrophe like a respiratory disease pandemic such as Covid-19 inflicts (and probably will inflict in future) upon billions of human beings, such a scientific endeavor is probably required more than ever before. It is to be recognized that this opinion article is not a comprehensive review of
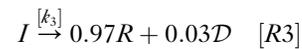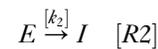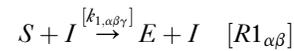
the Covid-19 disease spread; it is inherently biased toward a physical science—based viewpoint of the disease transmission problem, with a focus on the recent experiences and works of the authors. We hope the readers will pardon such a bias in view of the interdisciplinary connections that the approach attempts to achieve: connecting an epidemiological model with the science of colloidal suspension of virus particles in respiratory liquids along with the spatiotemporal interfacial processes of respiratory droplet evaporation and their conversion to droplet nuclei. For a comprehensive review of the state of the art, the readers can refer to the review article by Pöhlker et al. [12].

Physics-based disease spread model

Ironically, the first mathematical model for infectious disease spread was formulated by the mathematician/fluid dynamicist Daniel Bernoulli in 1760 [13,14], leading to the Kermack—McKendrick model in 1927 [15]. Since then, epidemiological models have evolved in great sophistication and complexity [16]. Mean-field compartmental models can lack the heterogeneity information in terms of population mobility and density—this has led to development of network models [17] and agent-based models [18] that attempt to model human mobility using different techniques such as complex networks and mobile agents, respectively. In parallel to the population dynamics viewpoint,

epidemiological model such as the Susceptible, Exposed, Infectious, Recovered, Deceased (SEIRD) model could be viewed as a chemical reaction mechanism. Here, the reaction is the infection transmitting from infected I individuals to susceptible individuals S who are converted to exposed E. Subsequently, E can become recovered R or deceased $\mathcal{D}$.

As shown in the study by Chaudhuri et al. [23],

$$S + I \overset{[k_{1,\alpha\beta\gamma}]}{\rightarrow} E + I \quad [R1_{\alpha\beta}]$$

$$E \overset{[k_2]}{\rightarrow} I \quad [R2]$$

$$I \overset{[k_3]}{\rightarrow} 0.97R + 0.03\mathcal{D} \quad [R3]$$

Here, the k_is are the rate constants of the corresponding 'reactions.' α corresponds to the particular expiratory event such as breathing, coughing, singing, sneezing, or talking, whereas β corresponds to the specific vector of transmission such as respiratory droplets (all possible sizes, thereby including both large and small droplets — the latter often referred to as aerosols in the transmission literature), droplet nuclei (typically aerosols), or fomites. γ corresponds to the specific location where the infection is occurring. The reaction [R3] assumes a 97% recovery rate

Figure 1
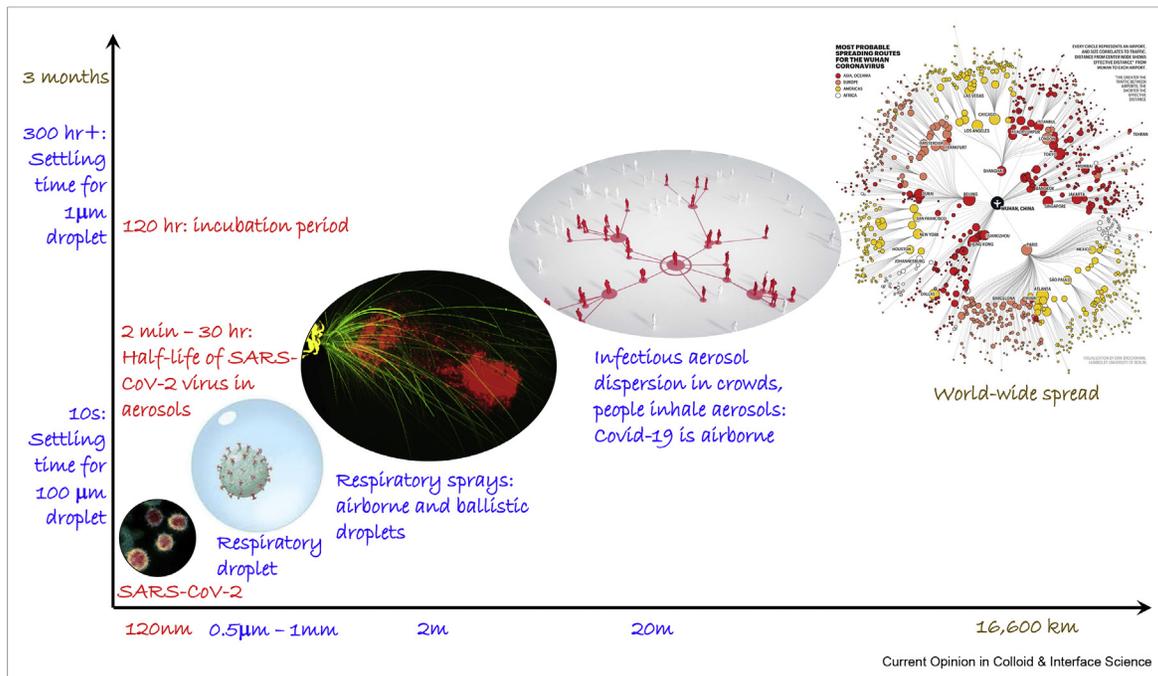
Multilength scale, multitime scale, multidisciplinary nature of the Covid-19 disease spread. Subimages adapted from [19–22]. Covid-19, coronavirus disease 2019; SARS-CoV-2, severe acute respiratory syndrome coronavirus 2. The cough image credit: Prof. Bourouiba, MIT/HHMI [20]. World-wide spread image credit: D. Brockmann, Humboldt University of Berlin [21].

and 3% mortality rate, respectively. Probability distributions of $k_{1,\alpha\beta\gamma}$ could be obtained, from which an appropriate statistic representing mean-field k_1 serving as the critical parameter for the corresponding mean-field disease spread Eqn. (1), for example, over a city could be derived. Alternatively, a network model could be used wherein the following ODE could be solved at different nodes of a network, in a network model. The mean-field ODE with the representative mean-field k_1 is shown as follows:

$$\frac{d[I]}{dt} = k_2[E] - k_3[I]$$
$$\frac{d[E]}{dt} = k_1[I][S] - k_2[E]$$
$$\frac{d[R]}{dt} = 0.97k_3[I] \qquad (1)$$
$$\frac{d[\mathcal{D}]}{dt} = 0.03k_3[I]$$
$$[S] + [E] + [I] + [R] + [\mathcal{D}] = 1$$

[] represents the respective fraction of the population. The skeletal structure of the SEIR model presented previously is well known. So, what has been achieved? What we get by casting the SEIR model in the form of a chemical reaction mechanism is that now the rate constant, k_1, can have a sound physical interpretation and thus paves the way for a first principles model. The rate constants k_2 and k_3 are controlled by the virus−human body (virology and physiology) interaction and can be assumed constants to a first approximation, whereas for a Covid-19−type infectious respiratory disease, k_1 is primarily controlled by the flow physics of human exhalations, virus kinetics, and statistics of human interactions. In chemical reaction mechanisms involving gas-phase reactions, the Arrhenius rate constants have been historically derived using collision theory and later by more sophisticated transition state theory [24]. Quantum mechanical modeling using density functional theory [25] has proved pivotal in estimating the structure of the transition states and the resulting potential energy landscapes. If quantum mechanics can be used to calculate rate constants of chemical reaction mechanisms, could the fluid mechanics of aerosols that fundamentally underpins the disease transmission of Covid-19 be used to obtain the rate constants of the SEIR model? Indeed, the challenges in obtaining such a rate constant from first principles are many, the first being that infection does not occur in a fixed environment with fixed physical dimensions. Human behavior even collectively may not be predictable. In such a scenario, a possible approach could be as follows: First, estimate the local rate constant $k_{1,\gamma}$ from $k_{1,\alpha\beta\gamma}$ for an idealized, yet sufficiently generalized and well-defined, condition. Once that is obtained, a distribution of such rate constants could be obtained for the different situations involved. The mean and/or other relevant statistics could be obtained from the corresponding moments of the resulting probability density functions to yield the mean-field k_1.

Covid-19 has been recognized as an airborne disease [26,27], although the ballistic droplet and fomite route could provide non-negligible transmissions. There are several studies that analyzed large-scale transmission events, which could not have occurred unless the virus was airborne. In particular, the Skagit Valley Chorale superspreading event [28], outbreak in a Guangzhou restaurant [29], and the Diamond Princess cruise ship [30] are some prominent examples wherein the infected cases were at a sufficient distance from the index case to be explained by the ballistic droplet or fomite route of transmission. As such, Lednicky et al. [31] could isolate severe acute respiratory syndrome coronavirus 2 (SARS-CoV-2) from aerosols collected 2−4.8 m from Covid-19−positive patients. One of the most influential theoretical contributions in estimating the probability of indoor infection by airborne disease is by Riley et al. [32] and is given by the Wells−Riley equation.

$$\mathcal{P} = 1 - e^{(-Ipqt/Q)} \qquad (2)$$

Here, $\mathcal{P}$ is the probability of infection, I is the number of infected individuals, p is the rate of breathing per person, q is the quantum (of infection) generation rate by I, t is the exposure time, and Q is the volume flow rate of incoming air. Rudnick and Milton [33] extended this further to define

$$\mathcal{P} = 1 - e^{-\mu t} \qquad (3)$$

Here, $\mu = \bar{f}Iq/n$ and $\bar{f}$ are the average fraction of indoor air that is exhaled as breadth and n is the number of people present in the space. From this, they derived the 'reproductive number for an infectious disease in a building environment' as

$$\mathcal{R}_{0A} = (n-1)e^{(\bar{f}Iqt/n)} \qquad (4)$$

This can be readily converted into k_1 of Eqn. (1). As such, this formulation has been extensively used as in the study by Buonanno et al. [34] to estimate the number of new infections and is a powerful tool to estimate infection risks. However, inherent in the simplicity, such a formulation has the following limitations embedded through its assumptions. (i) Spatially homogeneous aerosol concentration: While this assumption eliminates the need for flow physics considerations, it is a rather restrictive assumption because aerosols are exhaled from specific sources (of very small dimensions compared with room size) and mostly

disperse by turbulent diffusion. For continuous periodic activity such as breathing, even in steady state, it is unlikely that the aerosol concentration will be homogeneous in an indoor space at any time. Infectious aerosols will be much more concentrated close to the infected individual than in a remote corner of a room. If it were, any necessity of social distancing would be meaningless. As such, Chen et al. [35] emphasized the importance of a short-range airborne route dominated by small droplets in close-contact (<2 m) disease transmission. (ii) Absence of consideration of size distribution of aerosols: This also has an important bearing because larger sized droplets continuously settle, smaller ones remain airborne for longer times, and the initial size distribution and the local thermal fluid conditions determine the fraction of the originally exhaled aerosol population that will remain airborne after a particular time from the exhalation event. (iii) Absence of droplet physics and virus kinetics: SARS-CoV-2 has a half-life that can range from minutes to hours, in aerosols, depending on the local thermodynamic conditions and level of UV irradiation. The virus half-life could well be dependent on the chemical and/or thermodynamic state of the respiratory droplet or droplet nuclei. The aforementioned second and third limitations could be however addressed in modified forms of the Wells–Riley model as has been recently done by Parhizkar et al. [36]. An alternative analysis
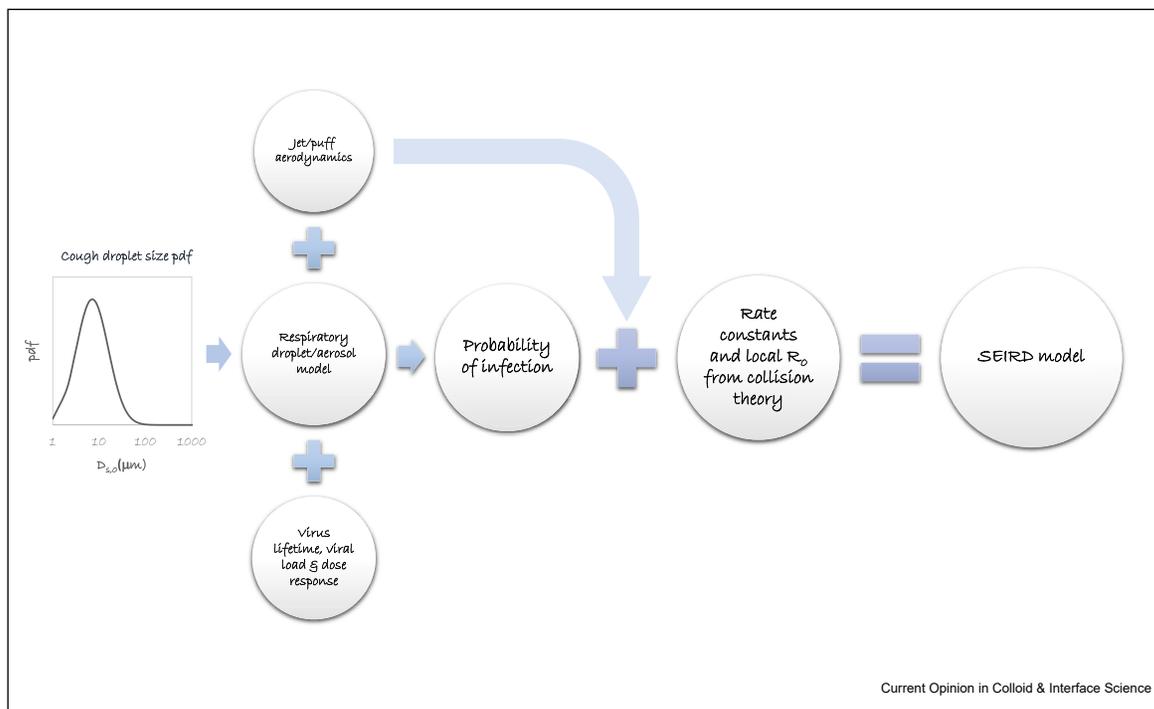
approach could be to estimate the basic reproduction number directly from the flow physics of exhalations starting from the exhaled respiratory droplet size distribution, drawing inspiration from the rate constants of chemical reactions. Indeed, such an approach is more complex, which often involves idealizing assumptions and involves subdisciplines ranging from turbulent dispersion to virus kinetics in evaporation of respiratory droplets. More importantly, instead of assuming a dominant pathway (aerosols), could an analysis be performed such that the dominant pathway emerges from the analysis itself? The structure and building blocks of such an analysis, adopted by Chaudhuri et al. [36] is shown in Figure 2.

Table 1

Infection rate constants for different expiratory events and modes of transmission (adapted from the study by Chaudhuri et al. [23]).

$k_{1,\alpha\beta}$	Droplet	Nucleus	Fomite
Breath	$k_{1,bd}$	$k_{1,bn}$	$k_{1,bf}$
Cough	$k_{1,cd}$	$k_{1,cn}$	$k_{1,cf}$
Sing	$k_{1,gd}$	$k_{1,gn}$	$k_{1,gf}$
Sneeze	$k_{1,sd}$	$k_{1,sn}$	$k_{1,sf}$
Talk	$k_{1,td}$	$k_{1,tn}$	$k_{1,tf}$

Figure 2

The overall model structure as an assembly of several interacting submodels. SEIRD: Suscetible, Exposed, Infectious, Recovered, Deceased.

Analyzing airborne pathways

Involving several idealizing assumptions and simplifications, the rate constants required for solving Eq. (1) and a basic reproduction number estimate starting from Duguid's [37] cough droplet size distribution were obtained by Chaudhuri et al. [23], a schematic of the model structure is shown in Fig. 2. Distributions of different parameters were not considered in this work although the sensitivity of the viral load on the rate constants was shown. Here, only the basic ideas are described. Drawing inspiration from molecular collision theory, the rate constants $k_{1,\alpha\beta}$ for each exhalation event α (breath, cough, sing, sneeze, or talk) and transmission vector β (droplets, droplet nuclei, or fomites as shown in Table 1) appearing in Eqns. [$R1_{\alpha\beta}$] could be derived as a function of the collision volume, probability of infection, and concentration of I and S individuals. The following paragraph shows how.

Let us assume that in a unit volume, the number of infected and susceptible individuals is n_I and n_S, respectively. Therefore, the number of collisions that would occur between the exhaled, infectious gas cloud $\mathbb{D}$ (ejected by I), and the susceptible individuals S is $V_c n_I n_S$. V_c is the collision volume, which is the volume swept by a cylinder of diameter $\sigma_{DS} = (\sigma_D + \sigma_S)/2$ in unit time. Here, σ_S is the diameter of the hemispherical, inhalation volume $\mathcal{V}_b = (1/12)\pi\sigma_S^3$, whereas σ_D is the diameter of the aerosol cloud that grows in time. When the aerosol cloud volume is less than the total volume under consideration and when the relative velocity between $\mathbb{D}$ and S is nonzero and given by V_{DS}, the frequency of collision Z is given by $\pi\sigma_{DS}^2 V_{DS} n_I n_S$. However, all collisions will not result in infection because the probability of infection $\mathcal{P}_{\alpha\beta}$ (for expiratory event α and transmission vector β) upon collision between S and $\mathbb{D}$ varies between 0 and 1. Including that, Chaudhuri et al. [23] defined the generalized rate constant by Eqn. 5

$$k_{1,\alpha\beta\gamma} = \frac{\pi n_{total,\gamma}}{t_c} \int_0^\tau \sigma_{DS}^2(t) V_{DS}(t) \mathcal{P}_{\alpha\beta}(t) dt \qquad (5)$$

where $n_{total,\gamma}$ is the number density (number/volume) of the inhalation volumes at a location γ. Given the variation in the height of the susceptible individuals, we assume the inhalation hemispheres (of volume $\mathcal{V}_b$) are uniformly distributed within a given vertical distance $\mathcal{H}$. If so, the population density $n_{density,\gamma}$ (number of people/area) could be converted to $n_{total,\gamma} = n_{density,\gamma}/\mathcal{H}$. This also explains why a collision volume and not a collision area has been considered. t_c is the average time period between two expiratory events.

Indeed, the rate constant $k_{1,\alpha\beta\gamma}$ is location, expiratory event specific, whereas the ones required for solving Eqn. (1) arises from a mean-field approximation. This can be addressed by (i) considering actual distributions of $n_{total,\gamma}$ and other relevant parameters (such as the viral load) in Eqn. (5) or (ii) constructing a network model wherein $k_{1,\alpha\beta\gamma}$ is calculated at individual locations, after summing it over α, β.

In Eqn. (5), probability of infection $\mathcal{P}_{\alpha\beta}$ upon crossing the droplet cloud $\mathbb{D}$ is a key term. Its practical importance also cannot be overstated. Most works used the 'quanta' of infectious emissions to estimate the probability of infection. Approximating Duguid's cough droplet size distribution with a log-normal distribution $f_\alpha(D) = \frac{1}{\sqrt{2\pi}\sigma D} exp[-(\ln(D) - \mu)^2/2\sigma^2]$, the number of virions within droplet sizes D_1 and D_2 is given by $N_{v\alpha} = \frac{\pi\rho_v N_{t\alpha}}{6} \int_{D_1}^{D_2} D^3 f_\alpha(D) dD$. Incorporating the virus kinetics for the transmission vector β by $\psi_\beta(t) = (1/2)^{t/t_{\beta\frac{1}{2}}}$, Chaudhuri et al. [23] calculated the number of virions that would be inhaled from droplets upon crossing the aerosol cloud $\mathbb{D}$ by

$$\mathcal{N}_{\alpha d}(t) = \frac{\pi\rho_v N_{t\alpha} N_b \sigma_S^3 (\sigma_S + \sigma_D(t))\psi_d(t)}{12 V_{DS}(t)\sigma_D^3(t)} \int\limits_{D_1(t)}^{D_2(t)} D^3 f_\alpha(D) dD$$

$$(6)$$

and the number of virions that would be inhaled from the dried droplet nuclei by

$$\mathcal{N}_{\alpha n}(t) = \frac{\pi\rho_v N_{t\alpha} N_b \sigma_S^3 (\sigma_S + \sigma_D(t))\psi_n(t)}{12 V_{DS}(t)\sigma_D^3(t)} \int\limits_{0}^{D_n(t)} D^3 f_\alpha(D) dD$$

$$(7)$$

where ρ_v is the viral load and $N_{t\alpha}$ is the number of respiratory droplets ejected. $\psi_\beta(t)$ is the fraction of infectious virions available at time t in the vector β, with $t_{\beta\frac{1}{2}}$ being the corresponding half-life of the virus. The limits of the integrals in Eqns. (6) and (7) are the initial droplet diameters that evaporate and settle at time t, respectively, and can be estimated from a modified Wells' plot wherein droplet evaporation and settling times are calculated accounting from the accompanying warm and moist air jet that is exhaled. The settling time is obtained from the Stokes terminal velocity accounting for droplet size reduction due to evaporation. The droplet size reduction due to evaporation and the heat transfer to/from the ambient can be modeled using an energy balance equation. Here, the droplet was assumed to be homogeneous. It has been shown that the effect of solute (nonvolatile components: mostly salts in respiratory fluids) concentration in the respiratory droplets is critical in predicting the accurate droplet lifetime [38]. This was incorporated in the model by tracking the overall solute concentration in the droplet. Its effect on the evaporation rate was included by evaluating suppression of vapor pressure of the evaporating species (water, here) as prescribed by Raoult's law. The translation of the droplet in the gas phase was modeled

using the 1D drag equation. This approach leads to a set of linear differential equations that can be simultaneously solved to estimate the temporal evolution of location, size, and temperature of the respiratory droplet. Such an approach readily incorporates effects of the ambient condition (temperature, humidity) and initial droplet size on the evaporation rate and final size of the nuclei. A detailed version of this model has been described by Chaudhuri et al. [23,39]. From these, the total probability of infection for the expiratory event α could be defined using the dose−response model:
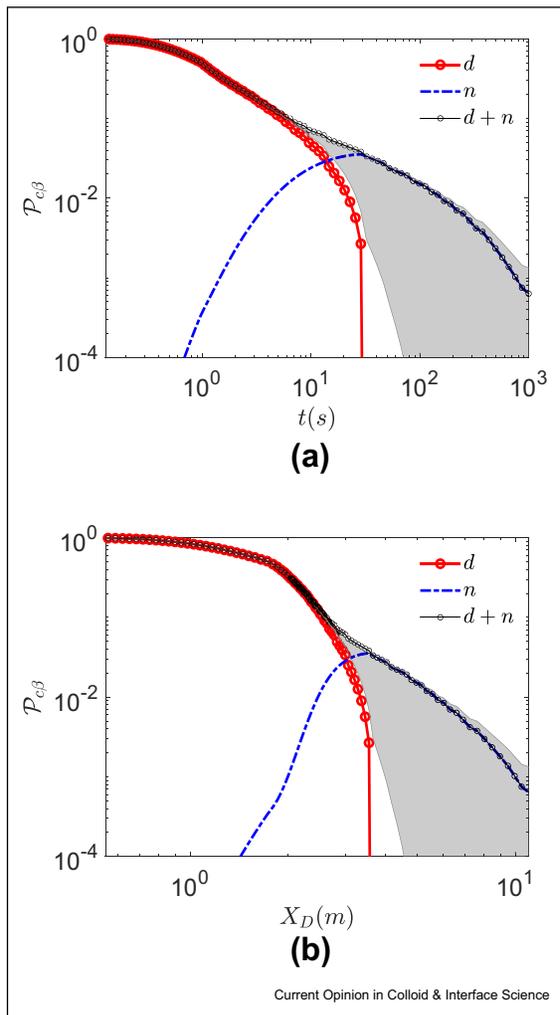
Figure 3

This figure shows probability of infection $\mathcal{P}_{c\beta}$ for the droplet route d and dried droplet nuclei route n, as well as total probability $\mathcal{P}_{\beta}$ while crossing the exhaled cloud for **(a)** as a function of time from the instant of the beginning of a single cough and **(b)** as a function of distance from location of the single cough along the center of the jet/puff trajectory. Note both d and n routes are essentially inhalation routes because large droplets settle in a very short time and are unlikely to contribute much in the disease transmission. $T_\infty = 21.44^oC$, $RH_\infty = 50\%$. The bold lines represent $\rho_v = 7 \times 10^6$ copies/ml with $t_{d\frac{1}{2}} = t_{n\frac{1}{2}} = t_{\frac{1}{2}}$, where $t_{\frac{1}{2}} = 15.25$ minutes. The gray-shaded region denotes the lower limit $t_{n\frac{1}{2}} = 0.01 t_{d\frac{1}{2}}$ and upper limit $t_{n\frac{1}{2}} = 100 t_{d\frac{1}{2}}$, respectively, with $t_{d\frac{1}{2}} = t_{\frac{1}{2}}$. Adapted from the study by Chaudhuri et al. [23].

$$\mathcal{P}_{\alpha}(t) = 1 - e^{-r_v \sum_\beta \mathcal{N}_{\alpha\beta}(t)} \qquad (8)$$

The aforementioned dose−response model is inspired by the seminal work of Haas [40]. The most important highlight of the combined system of Eqs. (6)−(8) is that here probability of infection is directly from the exhaled respiratory droplet size distribution without invoking 'quanta', as in previous studies. Of course, the individual probability of infection by the droplet route d and the dried droplet nuclei route n could be calculated. For a nonventilated large indoor space at a typical air-conditioned state, the results for a single cough are shown in Fig. 3.

Such an analysis can answer three fundamental questions quantitatively with corresponding uncertainty:

1. Why and how does the probability of infection reduce with time and distance from the source? The reason why $\mathcal{P}_{\alpha\beta}$ reduces with time and distance is due to (i) dilution of the aerosol cloud $\mathcal{D}$ by continuous entrainment of ambient air as captured by increasing $\sigma_D(t)$ with time (ii) droplet settling and evaporation if considering the droplet route reducing range within D_1 and D_2. But then, the droplet evaporates to produce droplet nuclei, which can remain infectious (iii) finite lifetime of the virus in droplets/droplet nuclei. This is accounted in $t_{\beta\frac{1}{2}}$, which is a function of temperature, relative humidity, and UV index [41,42]. Although ventilation is not considered, a practical method to reduce infection probability is by increasing ventilation that would dilute the aerosol cloud even further alongside direct removal of the infectious aerosol particles.

2. Which is the most dominant route of transmission? Ostensibly from Figure 3, the airborne droplet route has higher yet decaying probability. However, what is embedded in the log−log plot is that although the droplet nuclei has a much lower probability to infect, in the absence of ventilation, it has much longer persistence. The time scale of its persistence is long enough and can match well with the lifetime of the virus in the aerosols. Summarizing, the d-route offers high infection probability over shorter time and distance, whereas the n-route causes lower probability of infection but over longer time and distance. These two factors make the airborne dried droplet nuclei a very potent agent (possible more than the airborne droplets) of transmission. The role of droplet nuclei in infectious respiratory disease transmission was first identified by Wells. As shown in the study by Chaudhuri et al. [23], the contribution of the dried droplet nuclei to the infection rate constant and the corresponding basic reproduction number is much

larger than the corresponding droplets. Of course, this is under the assumption that the virus lifetime is same in both the droplet or dried droplet nuclei. This uncertainty is also addressed in Fig. 3.

3. What makes Covid-19 an airborne disease? Of course, there is a very important biological aspect to this question that is beyond the scope of the article. In the framework of the analysis presented here, the factors that render the disease airborne are the following:

   (i) High viral load ρ_v: This allows a significant number of virions to be present within very small droplets/droplet nuclei that can float in air for a significant time and can be directly inhaled deep into the lungs. The effect of the different viral loads on the corresponding basic reproduction number $\mathcal{R}_{0,c}$ was also shown [23]. In particular, it is apparent from this analysis that order of magnitude variation in the viral load leads to order of magnitude variation on the corresponding basic reproduction number (overdispersion) causing superspreading events.

   (ii) Relatively small minimum infectious dose captured by r_v: For Covid-19, the infectious dose is believed to be around $100-1000$ copies, although an exact number remains eluding at this time. Based on the dose response analysis by Haas [43] in terms of plaque forming units, Schijven et al. [44] suggested 1440 RNA-dependent RNA polymerase copies of SARS-CoV are required for infection.

   (iii) $t_{\beta\frac{1}{2}}$ substantially large and of similar order as t_{settle} for small droplets and aerosols: The long half-life of the virus inside aerosol particles under most common indoor conditions allows the virus to be airborne. This is one of the most, if not the most, important parameters that qualify SARS-CoV-2 to be transmitted by the airborne route.

Colloid and interfacial science of disease spread

The previous discussion has made it amply clear that long-term fate of the pathogen in respiratory fluid is critical in understanding how long the virus remains potent and airborne and thus how fast the disease spreads. For Covid-19—type pandemics, naturally, we ask what happens to the pathogen during its transportation through respiratory droplets. Although a detailed answer involves chemical, biological, and virological aspects of the pathogen, many critical insights can be obtained from the interfacial dynamics between the pathogen and carrier droplets. In fact, for a mechanistic understanding of migration of these pathogens, one can assume them to be particles with fixed dimensions [45,46]. The dimension of most pathogens varies between hundreds of nanometers and a few micrometers, and their Stokes numbers in water-based solutions are small. Thus, their motion is primarily dictated by the flow patterns in the carrier droplet, the interfacial interactions, and their own motility, if any.

As identified before, the respiratory droplets and droplet nuclei (including both large droplets and aerosols) can adopt three modes of infection transmission: airborne, direct impact, and fomites. The hydrodynamics, evaporation, and flow structure inside a sessile droplet (fomite) are very different from an airborne moving droplet owing to the solid substrate present in the former. Such a dichotomy in hydrodynamics also creates a disparity in the migration of pathogens and their position in desiccated nuclei for these two modes. For sessile droplets, Deegan et al. [47,48] explained that the very well-known coffee ring structure formed by particles in evaporating sessile droplets arises from the strong

Figure 4
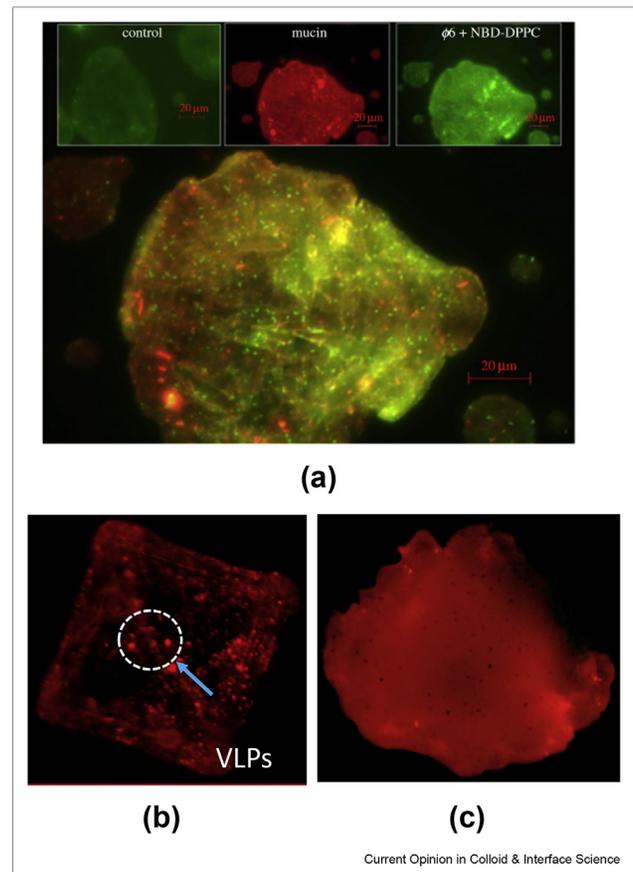
Drying of surrogate respiratory droplets. **(a)** Composite fluorescent image of the surrogate respiratory sessile droplet containing $\phi6$ virus exposed to 29% relative humidity. The bright green dots approximately 1 μm in size may indicate the location of the virus (adapted from the study by Vejerano and Marr [53]) **(b** and **c)** Fluorescent virus like particles (VLPs) inside the crystal formed in drying of the levitated droplet with a (b) two-component surrogate respiratory fluid compositions, 1% (w/w) aqueous NaCl solution (adapted from the study by Basu et al. [55]), and (c) four-component surrogate respiratory liquid, water, NaCl, DCCP, and mucin.

evaporation at the pinned contact line, which is supported by strong radially outward flow in the droplet close to the substrate. However, such an evaporating droplet also houses a couple of other effects including Marangoni and capillary flows, which can inhibit the formation of the coffee ring [49,50]. An evaporating sessile droplet with an unpinned contact line, on the other hand, can produce in general a more homogeneous distribution of particles on the substrate [51]. In a recent effort, Zhao and Yong [52] used a Lattice Boltzmann Method with Brownian dynamics to access the effects of nanoparticles at the liquid−vapor interface of an evaporating sessile droplet. While the number density of particles at the interface was found to influence the evaporation rate, the wettability played a strong role in accumulating the particles on the substrates. For weakly wettable surfaces, the particles were observed to be aggregated near the apex of the droplet, whereas for highly wettable substrates, they were accumulated near the contact line. A more homogeneous distribution was obtained for the neutral-wetting substrate.

While the underlined basic mechanism in particle deposition in water-based solutions explained in these studies can be extended to pathogens, the dynamics in respiratory droplets are more involved owing to the physicochemical complexities and the resulting variation in thermophysical properties. Vejerano and Marr [53] showed that the surrogate respiratory (sessile) droplets containing dissolved salts undergo an efflorescence process depending on the ambient relative humidity, which affects the crystallization process. Using a fluorescently tagged lipid, they could also isolate the virus locations in drying fomites at various ambient conditions. The salt (NaCl) in the respiratory droplets crystallizes on the substrate, whereas the other components (mucin, DPPC- dipalmitoylphosphatidylcholine) can form a shell-like structure, encapsulating the virus particles. Figure 4a shows the possible distribution of virus in a drying surrogate respiratory droplet with $\phi 6$ virus exposed in an ambient RH of 29%. In particular, they highlighted that some preferential chemical affinity in available active organic and inorganic groups in the solution of water, DPPC and NaCl, might expedite the process of shell/layer formation. Nevertheless, as the evaporation continues, eventually the nucleus of NaCl forms, leading to crystallization. In a more recent effort, Rasheed et al. [54] highlighted the effects of substrate characteristics on fomites' crystallization dynamics. They showed that dendritic or cruciform-shaped crystals were formed majorly for most substrates, but regular cubical crystals were observed for machined steel substrates.

The dynamics of pathogens in an airborne droplet are challenging to study experimentally owing to the involved complexity in isolating a single droplet in a controlled environment. An acoustic levitator, which can suspend a droplet by trapping it around a pressure antinode in a standing wave, paved the way for studying isolated droplets in container-less environments [56−61]. More recently, Basu et al. [55] used such a setup in studying the surrogate respiratory droplet containing virus-like particles (VLPs). They used 1% (w/w) NaCl aqueous solution as the surrogate respiratory fluid and 100-nm fluorescent particles as a surrogate virus, whose concentration was modulated from 0.005% to 0.1%. Although the chemical and biological signatures cannot be replicated, these VLPs can mimic the hydrodynamics of SARS-CoV-2. The study confirmed that, irrespective of the initial droplet diameter and the concentration of VLPs, the respiratory droplets evaporate and desiccate to form nuclei which are 20−30% of the initial droplet diameter in size. Importantly, they identified that at 50% RH, the desiccated nucleus consists of a single NaCl crystal containing the VLPs. The detailed confocal scanning of the crystals located a large portion of VLPs is in the crystal's inner core, whereas the rest of them were distributed in the outer edges and on the surfaces on the crystal. The VLP's and NaCl's relative diffusivities were compared with the droplet regression rate to demonstrate that, while homogeneity in fast-moving NaCl concentration was expected in the levitated respiratory droplet, VLPs were expected to be preferentially accumulated. Furthermore, the vortical motion created inside either levitated [61−63] or airborne droplets [64] induces the preferential distribution of VLPs mentioned previously. Figures 4b and c show the final precipitates and VLP distribution in levitated respiratory droplets at an RH of 50% using two different surrogate droplet recipes. The study was then extended to actual human saliva, collected from various uninfected healthy subjects. While the variation of saliva content, arising from the subjects' eating, drinking, and physiological habits, resulted in a large scatter in the data, the average behavior closely followed the trend predicted with surrogate respiratory liquid. A similar study for a broader range of ambient conditions was reported recently by Lieber et al. [38], who also observed similar evaporation dynamics.

Direct assessment of SARS-CoV-2 kinetics (infectivity) in aerosols and in sessile droplets has been reported by Schuit et al. [41] and Lin and Marr [65] and by Metcalf et al. [8], respectively. All studies found that SARS-CoV-2 stability monotonically decreases with increase in temperature. Morris et al. [66] reported a U-shaped virus half-life behavior with ambient relative humidity. They attributed such response to the solute concentration in the respiratory droplets. Consistent with previous findings by Marr et al. [67], enveloped viruses such as SARS-CoV-2 survives well in droplets far from their dried state, as well as in the desiccated residue, where the virus remains in a frozen state. In intermediate relative humidity levels (40−60%), in partially

dried equilibrated droplets with highest solute concentration, the virus survives for the least time, with all other conditions being held equal. Indeed, virus survivability within desiccated nuclei enables the virus to be airborne.

Disease prevention: face masks

Analysis presented in Analyzing airborne pathways can be used to understand the effect of blocking droplets of different sizes on the probability of infection. Starting with Duguid's cough droplet size distribution, it has been shown that preventing ejection of all droplets larger than the initial size of 10 μm can substantially reduce the probability of infection [23]. Furthermore, it was also shown that preventing ejection of droplets larger than 5 μm could result in a two order of magnitude reduction in the $\mathcal{R}_{0,c}$ to a $\mathcal{R}_{0,c} < 1$ even for a very high viral load of $\rho_V = 2.35 \times 10^9 copies/ml$. Large $\mathcal{R}_{0,c}$ are characteristics of superspreader events; therefore, blocking respiratory droplets up to a very small size such as 5 μm could ideally mitigate such events. Clearly, such physical blockage of respiratory droplets at the point of source could be accomplished with high-quality, well-fitted face masks. Face masks provide a physical obstruction to respiratory droplets, and their effectiveness in restricting droplet penetration depends on the effective pore size. Among the several local and medical-grade options available on the market, N95 masks are proven to be most effective. However, for community usage, their scarcity and high cost during the pandemic have diverted the policymakers to look for other economic and easily accessible alternatives such as surgical masks, cotton masks, or homemade face masks. Historically, the usage of the face mask has been shown effective in restricting transmission of pulmonary tuberculosis (aerosol-based) and influenza (droplet-based)-based illnesses and restricting community transmission in Asian countries during the SARS-CoV-1 epidemic [68]. Face masks are therefore useful in obstructing respiratory droplets during exhalation and inhalation and must be used ubiquitously to restrict the transmission of Covid-19.

Although all face coverings provide some protection, their relative efficacy depends on the type of mask used. Several studies [69–73] have been carried out in recent times, focusing on investigating mask efficacy. Fischer et al. [69] used a laser-based optical measurement technique to determine the effectiveness of different locally available face coverings (compared with no face covering) in restricting ejected droplets during human speech. Homemade substitutes (such as cotton masks) had equivalent effectiveness as that of surgical face masks, and compared with no mask, they were found to restrict ∼80% of droplets from penetration. At the same time, some other substitutes such as bandanas or neck gaiters have shown low or minimal protection. Hui et al.

[74] used a high-fidelity human patient simulator lying at 45° on a hospital bed for investigating the distance traveled by cough puffs when the human patient simulator was covered with no mask, surgical masks, and N95 face masks. The velocities of ejected coughs were varied by controlling the flow rate of ejected fluid from 220 to 650 l/min, which resulted in maximum cough velocities of around 8 m/s. The turbulent cough flow without a mask was shown to traverse up to 70 cm, and the distance traveled reduces by a factor of 2.3 and 4.5 with the usage of surgical and N95 face masks, respectively. The N95 mask effectively reduced the translational displacement of the ejected cough, but a significant transverse leakage was observed. Recently, Khosronejad et al. [75] numerically studied the effectiveness of face masks in indoor environments and showed that saliva droplets ejected during coughs in a stagnant environment without a mask could reach a distance of 2.62 m, and the same distance reduces to 0.48 m and 0.78 m for medical and nonmedical grade face masks. They also emphasized that under the influence of mild unidirectional breeze in the outdoor environment, saliva particulates can travel long distances in the flow direction in a short period, and face mask usage in such situations is necessary for preventing the inhalation of these droplets.

Earlier works on face masks mostly focused on determining filtration efficiency, comparing different types of medical grade and makeshift masks, and investigating the distance traveled by the ejected cough puff and the capability of the face mask in restricting it. These investigations were mainly carried out on small-sized cough droplets (∼0.1−100 μm) that can be easily transmitted or show minimal atomization during their passage through the mask layers. It must be noted that droplets (submicron to millimeter sizes) across a wide size range are generated during human coughs. Among these droplets, the larger sized droplets (>250 μm) are less in number but contribute to 90% of the ejected volume [73]. Because the viral loading inside the droplet is volumetric, considering the fate of such large-sized droplets during their impact on the mask surface becomes essential. The large-sized droplets usually settle on the ground within seconds under the influence of gravity. However, on impacting a mask surface higher than certain threshold velocities, these droplets undergo atomization into numerous tiny daughter droplets, most of which fall under the critical regime of aerosolization (<100 μm) [73]. This mechanism showed that the risk of infection through this route might be higher than what is predicted by considering mask filtration efficiencies alone. An experimental study in this direction was recently carried by Sharma et al. [73], which uncovers the evolution of a large-sized cough droplet during its impingement on single-layer or multilayer face masks. The aspects of droplet penetration, atomization mechanism, and final size distribution were

elucidated using side-view shadowgraphy imaging, and the experimental results of droplet penetration and atomization were also validated using an existing theoretical framework.

During this study, the primary experiments were conducted using surrogate cough droplets of the size (D_i) ~ 620 μm ejected at ~ 10 m/s (typical for a cough droplet) and impacting on a single-, double-, or triple-layer surgical face mask. Figure 5a schematically shows the atomization of a virus such as particle-laden surrogate cough droplet while impacting the mask surface. Owing to high impact velocity and Weber number ($We = \rho_w v_i^2 D_i / \sigma \sim 50$ at penetration threshold), the inertia of the droplet dominates over surface tension forces, and thus, the surface tension effects on the phenomenon were negligible. The impacting droplet penetrates through the mask layers if the kinetic energy of the impacting droplet overcomes the energy loss owing to viscous dissipation during liquid flow through the porous network of the mask. This penetration criterion was established in the study by Sahu et al. [76] and was validated experimentally for different droplet impact velocities ($v_i \sim 2-10$ m/s) and droplet diameters ($D_i = 250-1200$ μm) [73]. It was shown that penetration of the droplet through the face mask is independent of the impacting droplet diameter, provided the effective pore size (ε) of the mask is much smaller than the droplet size (D_i), that is, $\varepsilon \ll D_i$, which was indeed the case during experiments. The penetration of the droplet through the different layered masks is shown in Figure 5b. For a single-layer mask, the impacting droplet extrudes through the mask layer in the form of multiple cylindrical ligaments that grow in length over time, because of which instabilities in the form of capillary waves are formed on the surface of the ligaments. The growth of these instabilities leads to the atomization into numerous tiny droplets. The estimation of droplet size and breakup time based on Rayleigh−Plateau instability criteria was performed and shown to be in good match with the experimental data (refer to the study by Sharma et al. [73]). The results showed that thicker ligaments lead to bigger droplet sizes and longer breakup times, and vice versa. During droplet penetration through double- or triple-layer masks, the ligament formation was not observed owing to the obstruction provided by the multiple layers of the mask. The extent of penetration was less through a double-layer mask, and no droplet or single-droplet penetration was observed through a triple-layer mask (see Fig. 5b).

The size distribution of atomized droplets is shown in Figure 1c, and the blue region in this curve indicates the droplet sizes <100 μm, which have a higher aerosolization tendency and is referred to as a critical regime. The majority of atomized droplets lie in a critical regime for both single-($\sim 60\%$) and double-layer ($\sim 80\%$) face masks. Each experimental run resulted in penetration of ~ 110 and ~ 20 droplets (which corresponds to $\sim 65\%$ and $\sim 5\%$ of the initial volume) for single- and double-layer masks. Although the number counts of penetrated droplets differ for single- and double-layer masks, the probability distribution of atomized droplets remains similar for both masks. To consider the difference in fluid properties of de-ionized (DI) water droplets and actual cough droplets (containing dissolved salt and proteins), experiments were also carried out with surrogate respiratory fluid. Similar results of droplet size distribution and penetration volume percentage were observed for this case (refer to the study by Sharma et al. [73]). This indicates that the penetration and

Figure 5

Current Opinion in Colloid & Interface Science
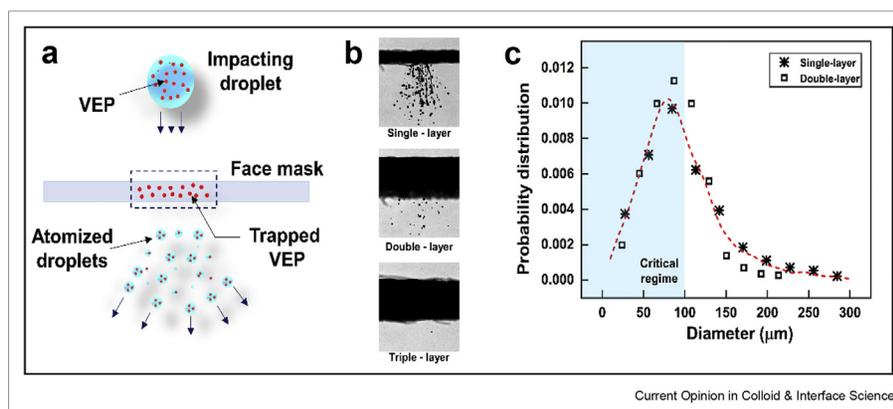
Secondary atomization of cough droplets through a face mask. **(a)** Schematic diagram representing atomization of impacting the droplet into numerous daughter droplets after penetration through the face mask. **(b)** Experimental images showing the extent of penetration through single-, double-, and triple-layer face masks (from top to bottom in sequence). **(c)** Probability distribution for the diameter of atomized droplets showing most daughter droplets lie in the critical regime (figure adapted from the study by Sharma et al. [73]). VEP, Virus emulating particles.

atomization of high-impact velocity droplets through the face mask is independent of fluid properties. Additional experiment results with variable impact velocities ($3-10$ m/s) and impact angles ($45°$ and $60°$) were also demonstrated to bolster further this study's relevance with droplet atomization scenarios during human coughs. It was shown that at higher impact velocities ($7-10$ m/s) and different impact angles, no significant difference in the daughter droplet size distribution and penetrated volumes was observed (refer to the study by Sharma et al. [73]). In conclusion, a single-layer mask that restricts 30% of the droplet volume was shown to be least effective in the study. A double-layer mask was more effective and obstructs $\sim 91\%$ of droplet volume, but 27.7% of transmitted volume falls in the critical regime, and at least a triple-layer mask is recommended for which only single-droplet or no droplet penetration was observed. It must also be noted that any face covering, even a single-layer face mask, provides some resistance to exhaled respiratory droplets during human coughs and, as such, should be used whenever required and mandated by policymakers.

Conclusions

In this article, we have provided an opinion on the need and the possible approach to develop a multiscale physics-based disease spread model from first principles. This is an ambitious goal and an ongoing endeavor. Such an effort is inherently multidisciplinary in that one has to combine expertise of aerosol scientists, fluid dynamicists, virologists, and interfacial scientists under one common umbrella to develop such models that can be used for any respiratory disease transmission for any viral outbreak. We have shown in detail that chemical kinetics—based pandemic model can be coupled with droplet-level physics inclusive of evaporation, dispersion, and precipitation to devise a hitherto new methodology to predict the infection spread in the context of Covid-19. In particular, we also showed how the model can be improved by incorporating viral load distribution and kinetics by using novel experimental techniques. Furthermore, the model can consummate new physics derived from social prevention measures such as masks and social distancing. On a related topic, unique atomization pathways of cough droplets in single- or double-layer masks were investigated. We finally harp the importance of a first principles model well validated by experiments as a cornerstone of any pandemic macro-scale model in the near future.

Declaration of competing interest

The authors declare that they have no known competing financial interests or personal relationships that could have appeared to influence the work reported in this paper.

References

Papers of particular interest, published within the period of review, have been highlighted as:

*   of special interest
** of outstanding interest

1. Li R, Pei S, Chen B, Song Y, Zhang T, Yang W, Shaman J: **Substantial undocumented infection facilitates the rapid dissemination of novel coronavirus (sars-cov-2)**. *Science* 2020, **368**:489–493, https://doi.org/10.1126/science.abb3221.

2. Gandhi M, Yokoe DS, Havlir DV: *Asymptomatic transmission, the achilles' heel of current strategies to control covid-19.* 2020.

3. Pullano G, Di Domenico L, Sabbatini CE, Valdano E, Turbelin C, Debin M, Guerrisi C, Kengne-Kuetche C, Souty C, Hanslik T, Blanchon T, Boëlle P-Y, Figoni J, Vaux S, Campèse C, Bernard-Stoecklin S, Colizza V: **Underdetection of covid-19 cases in France threatens epidemic control**. *Nature* 2020, https://doi.org/10.1038/s41586-020-03095-6.

4. Shaman J: *An estimation of undetected covid cases in France.* 2020. https://www.nature.com/articles/d41586-020-03513-9.

5. Subramanian R, He Q, Pascual M: **Quantifying asymptomatic infection and transmission of covid-19 in New York city using observed cases, serology, and testing capacity**. *Proc Natl Acad Sci USA* 2021, **118**.

6. Bertozzi AL, Franco E, Mohler G, Short MB, Sledge D: *The challenges of modeling and forecasting the spread of covid-19.* 2020. arXiv preprint arXiv:2004.04741.

7. Adam D: **Special report: the simulations driving the world's response to covid-19**. *Nature* 2020, **580**:316.

8. Metcalf CJE, Morris DH, Park SW: **Mathematical models to guide pandemic response**. *Science* 2020, **369**:368–369.

9. Moriyama M, Hugentobler WJ, Iwasaki A: **Seasonality of respiratory viral infections**. *Annu Rev Virol* 2020, **7**.

10. Fisman DN: **Seasonality of infectious diseases**. *Annu Rev Publ Health* 2007, **28**:127–143.

11. Shaman J, Kohn M: **Absolute humidity modulates influenza survival, transmission, and seasonality**. *Proc Natl Acad Sci USA* 2009, **106**:3243–3248.

12. Pöhlker ML, Krüger OO, Förster J-D, Elbert W, Fröhlich-Nowoisky J, Pöschl U, Pöhlker C, Bagheri G, Bodenschatz E, Huffman JA, *et al.*: *Respiratory aerosols and droplets in the transmission of infectious diseases.* 2021. arXiv preprint arXiv:2103.01188.

13. Bernoulli D: **Essai d'une nouvelle analyse de la mortalité causée par la petite vérole, et des avantages de l'inoculation pour la prévenir, Histoire de l'Acad**. *R Sci (Paris) Mem* 1760:1–45.

14. Dietz K, Heesterbeek J: **Daniel Bernoulli's epidemiological model revisited**. *Math Biosci* 2002, **180**:1–21.

15. Kermack WO, McKendrick AG: **A contribution to the mathematical theory of epidemics**. *Proc R Soc Lond - Ser A Contain Pap a Math Phys Character* 1927, **115**:700–721.

16. Keeling MJ, Rohani P: *Modeling infectious diseases in humans and animals.* Princeton University Press; 2011.

17. Pastor-Satorras R, Castellano C, Van Mieghem P, Vespignani A: **Epidemic processes in complex networks**. *Rev Mod Phys* 2015, **87**:925.

18. Ferguson NM, Cummings DA, Cauchemez S, Fraser C, Riley S, Meeyai A, Iamsirithaworn S, Burke DS: **Strategies for containing an emerging influenza pandemic in southeast asia**. *Nature* 2005, **437**:209–214.

19. National Institute of Health (NIH): *Novel coronavirus structure reveals targets for vaccines and treatments*. 2020. https://www.nih.gov/news-events/nih-research-matters/novel-coronavirus-structure-reveals-targets-vaccines-treatments.

20. Bourouiba L: *The Anatomy of a Sneeze, HHMI: Biointeractive*. 2016. https://www.biointeractive.org/classroom-resources/anatomy-sneeze.

21. Fortune: *Mapping a contagion: how the coronavirus may spread around the world*. 2020. https://fortune.com/longform/how-coronavirus-spread-map.

22. Bourouiba L: **Turbulent gas clouds and respiratory pathogen**
** **emissions: potential implications for reducing transmission of Covid-19**. *JAMA* 2020, **323**:1837–1838.
This recent review describes the trajectory of respiratory droplets and droplet-cloud after violent expiratory events. The work highlights that the droplet could initially behaves like a turbulent jet and subsequently, transforms to a turbulent puff.

23. Chaudhuri S, Basu S, Saha A: **Analyzing the dominant sars-**
** **cov-2 transmission routes toward an ab initio disease spread model**. *Phys Fluids* 2020, **32**:123306.
This work is probably the first attempt to develop a disease spread model from the flow physics of transmission. This is done by analyzing the relative importance of evaporating respiratory droplets and their dried droplet nuclei as function of distance and time from the subject, in the transmission of disease.

24. Law CK: *Combustion physics*. Cambridge University Press; 2006, https://doi.org/10.1017/CBO9780511754517.

25. Hohenberg P, Kohn W: **Inhomogeneous electron gas**. *Phys Rev* 1964, **136**:B864.

26. Prather KA, Marr LC, Schooley RT, McDiarmid MA, Wilson ME,
* Milton DK: **Airborne transmission of sars-cov-2**. *Science* 2020, **370**:303–304.
This is an important recent article which highlights proper definition of aerosol when it comes to respiratory droplet. The paper suggests that the respiratory droplets smaller than 100 micron should be called 'aerosols' since these droplets can remain airborne for much longer time and travel to long distances compared to the larger droplets.

27. Morawska L, Milton DK: **It is time to address airborne transmission of coronavirus disease 2019 (covid-19)**. *Clin Infect Dis* 2020, **71**:2311–2313.

28. Miller SL, Nazaroff WW, Jimenez JL, Boerstra A, Buonanno G, Dancer SJ, Kurnitski J, Marr LC, Morawska L, Noakes C: **Transmission of sars-cov-2 by inhalation of respiratory aerosol in the skagit valley chorale superspreading event**. *Indoor Air* 2021, **31**:314–323.

29. Li Y, Qian H, Hang J, Chen X, Cheng P, Ling H, Wang S, Liang P, Li J, Xiao S, *et al.*: **Probable airborne transmission of sars-cov-2 in a poorly ventilated restaurant**. *Build Environ* 2021:107788.

30. Azimi P, Keshavarz Z, Laurent JGC, Stephens B, Allen JG: **Mechanistic transmission modeling of covid-19 on the diamond princess cruise ship demonstrates the importance of aerosol transmission**. *Proc Natl Acad Sci USA* 2021, **118**.

31. Lednicky JA, Lauzard M, Fan ZH, Jutla A, Tilly TB, Gangwar M,
* Usmani M, Shankar SN, Mohamed K, Eiguren-Fernandez A, *et al.*: **Viable sars-cov-2 in the air of a hospital room with covid-19 patients**. *Int J Infect Dis* 2020, **100**:476–482.
This work provides the most important proof that Covid-19 is an airborne disease. Virus collected from significant distance from Covid-19 patients were successfully cultured.

32. Riley E, Murphy G, Riley R: **Airborne spread of measles in a suburban elementary school**. *Am J Epidemiol* 1978, **107**: 421–432.

33. Rudnick S, Milton D: **Risk of indoor airborne infection transmission estimated from carbon dioxide concentration**. *Indoor Air* 2003, **13**:237–245.

34. Buonanno G, Stabile L, Morawska L: **Estimation of airborne viral emission: quanta emission rate of sars-cov-2 for infection risk assessment**. *Environ Int* 2020:105794.

35. Chen W, Zhang N, Wei J, Yen H-L, Li Y: **Short-range airborne route dominates exposure of respiratory infection during close contact**. *Build Environ* 2020:106859.

36. Parhizkar H, Van Den Wymelenberg K, Haas C, Corsi R: **A quantitative risk estimation platform for indoor aerosol transmission of covid-19**. *medRxiv* 2021, https://doi.org/10.1101/2021.03.05.21252990.

37. Duguid J: **The numbers and the sites of origin of the droplets expelled during expiratory activities**. *Edinb Med J* 1945, **52**: 385.

38. Lieber C, Melekidis S, Koch R, Bauer H-J: **Insights into the evaporation characteristics of saliva droplets and aerosols: levitation experiments and numerical modeling**. *J Aerosol Sci* 2021:105760.

39. Chaudhuri S, Basu S, Kabi P, Unni VR, Saha A: **Modeling the role of respiratory droplets in covid-19 type pandemics**. *Phys Fluids* 2020, **32**, 063309.

40. Haas CN: **Estimation of risk due to low doses of microorganisms: a comparison of alternative methodologies**. *Am J Epidemiol* 1983, **118**:573–582.

41. Schuit M, Ratnesar-Shumate S, Yolitz J, Williams G, Weaver W, Green B, Miller D, Krause M, Beck K, Wood S, *et al.*: **Airborne sars-cov-2 is rapidly inactivated by simulated sunlight**. *J Infect Dis* 2020, **222**:564–571, https://doi.org/10.1093/infdis/jiaa334.

42. U. S. Department of Homeland Security, reportEstimated Airborne Decay of SARS-CoV-2; https://www.dhs.gov/science-and-technology/sars-airborne-calculator, Technical Report, URL: https://www.dhs.gov/science-and-technology/sars-airborne-calculator.

43. Haas C: *Action levels for sars-cov-2 in air: a preliminary approach*. 2020.

44. Schijven J, Vermeulen LC, Swart A, Meijer A, Duizer E, de Roda Husman AM: **Quantitative microbial risk assessment for airborne transmission of sars-cov-2 via breathing, speaking, singing, coughing, and sneezing**. *Environ Health Perspect* 2021, **129**, 047002.

45. Mushenheim PC, Trivedi RR, Tuson HH, Weibel DB, Abbott NL: **Dynamic self-assembly of motile bacteria in liquid crystals**. *Soft Matter* 2014, **10**:88–95.

46. Lauga E: **Bacterial hydrodynamics**. *Annu Rev Fluid Mech* 2016, **48**:105–130.

47. Deegan RD, Bakajin O, Dupont TF, Huber G, Nagel SR, Witten TA: **Capillary flow as the cause of ring stains from dried liquid drops**. *Nature* 1997, **389**:827–829.

48. Deegan RD, Bakajin O, Dupont TF, Huber G, Nagel SR, Witten TA: **Contact line deposits in an evaporating drop**. *Phys Rev E* 2000, **62**:756.

49. Hu H, Larson RG: **Marangoni effect reverses coffee-ring depositions**. *J Phys Chem B* 2006, **110**:7090–7094.

50. Yunker PJ, Still T, Lohr MA, Yodh A: **Suppression of the coffee-ring effect by shape-dependent capillary interactions**. *Nature* 2011, **476**:308–311.

51. Larson RG: **Transport and deposition patterns in drying sessile droplets**. *AIChE J* 2014, **60**:1538–1571.

52. Zhao M, Yong X: **Modeling evaporation and particle assembly in colloidal droplets**. *Langmuir* 2017, **33**:5734–5744.

53. Vejerano EP, Marr LC: **Physico-chemical characteristics of**
** **evaporating respiratory fluid droplets**. *J R Soc Interface* 2018, **15**:20170939.

This work describes a pioneering experiment to image and understand virus distribution inside dried droplet nuclei.

54. Rasheed A, Sharma S, Kabi P, Saha A, Chaudhuri S, Basu S: **Insights into the precipitation dynamics of surrogate respiratory sessile droplets leading to possible fomites**. *J Colloid Interface Sci* 2021, **600**:1−13.

55. Basu S, Kabi P, Chaudhuri S, Saha A: **Insights on drying and precipitation dynamics of respiratory droplets from the perspective of covid-19**. *Phys Fluids* 2020, **32**:123317.

56. Yarin A, Pfaffenlehner M, Tropea C: **On the acoustic levitation of droplets**. *J Fluid Mech* 1998, **356**:65−91.

57. Yarin A, Brenn G, Kastner O, Rensink D, Tropea C: **Evaporation of acoustically levitated droplets**. *J Fluid Mech* 1999, **399**: 151−204.

58. Saha A, Basu S, Suryanarayana C, Kumar R: **Experimental analysis of thermo-physical processes in acoustically levitated heated droplets**. *Int J Heat Mass Tran* 2010, **53**: 5663−5674.

59. Saha A, Basu S, Kumar R: **Effects of acoustic-streaming-induced flow in evaporating nanofluid droplets**. *J Fluid Mech* 2012, **692**:207−219.

60. Wei Y, Yang Y, Zhang J, Deng S, Liu S, Law CK, Saha A: **Atomization of acoustically levitated droplet exposed to hot gases**. *Appl Phys Lett* 2020, **116**, 044101.

61. Hasegawa K, Abe Y, Kaneko A, Yamamoto Y, Aoki K: **Visualization measurement of streaming flows associated with a single-acoustic levitator**. *Microgravity Sci Technol* 2009, **21**: 9−14.

62. Saha A, Basu S, Kumar R: **Particle image velocimetry and infrared thermography in a levitated droplet with nanosilica suspensions**. *Exp Fluid* 2012, **52**:795−807.

63. Saha A, Basu S, Kumar R: **Velocity and rotation measurements in acoustically levitated droplets**. *Phys Lett A* 2012, **376**: 3185−3191.

64. Sirignano WA: *Fluid dynamics and transport of droplet and sprays*. Cambridge University Press; 2010.

65. Lin K, Marr LC: **Humidity-dependent decay of viruses, but not**
* **bacteria, in aerosols and droplets follows disinfection kinetics**. *Environ Sci Technol* 2019, **54**:1024−1032.
This is another very important work that provides fundamental insights on how virus half-life is a non-monotonic function of relative humidity.

66. Morris DH, Yinda KCH, Gamble A, Rossine FW, Huang Q, Bushmaker T, Fischer RJ, Matson MJ, van Doremalen N, Vikesland PJ, *et al.*: **The effect of temperature and humidity on the stability of sars-cov-2 and other enveloped viruses**. *bio-Rxiv* 2020, https://doi.org/10.1101/2020.10.16.341883.

67. Marr LC, Tang JW, Van Mullekom J, Lakdawala SS: **Mechanistic**
** **insights into the effect of humidity on airborne influenza virus survival, transmission and incidence**. *J R Soc Interface* 2019, **16**:20180298.
This is an important publication that discusses effects of ambient humidity and temperature on air-borne virus lifetime. The paper also shows that relative humidity, not absolute humidity controls the evaporation rate of droplets and as such dictates virus lifetime.

68. Esposito S, Principi N, Leung CC, Migliori GB: **Universal use of face masks for success against covid-19: evidence and implications for prevention policies**. *Eur Respir J* 2020, **55**.

69. Fischer EP, Fischer MC, Grass D, Henrion I, Warren WS,
** Westman E: **Low-cost measurement of face mask efficacy for filtering expelled droplets during speech**. *Sci Adv* 2020, **6**. eabd3083.
A critical paper in assessing efficacy of various quality of facemasks used during Covid-19. The study develops a simpler measurement system to quantify the blockage ratio for a wide range of mask-types.

70. Dbouk T, Drikakis D: **On respiratory droplets and face masks**. *Phys Fluids* 2020, **32**, 063303.

71. Verma S, Dhanak M, Frankenfield J: **Visualizing the effectiveness of face masks in obstructing respiratory jets**. *Phys Fluids* 2020, **32**, 061708.

72. Kumar S, Lee HP: **The perspective of fluid flow behavior of respiratory droplets and aerosols through the facemasks in context of sars-cov-2**. *Phys Fluids* 2020, **32**:111301.

73. Sharma S, Pinto R, Saha A, Chaudhuri S, Basu S: **On secondary**
* **atomization and blockage of surrogate cough droplets in single- and multilayer face masks**. *Sci Adv* 2021, **7**, https://doi.org/10.1126/sciadv.abf0452.
This is a recent investigation on fate of cough droplets as they impact single- and multi-layer masks. The paper clearly identifies that a high momentum, large cough droplet penetrates single and double-layer facemasks producing many smaller aerosolized droplets.

74. Hui DS, Chow BK, Chu L, Ng SS, Lee N, Gin T, Chan MT: **Exhaled air dispersion during coughing with and without wearing a surgical or n95 mask**. *PloS One* 2012, **7**, e50845.

75. Khosronejad A, Santoni C, Flora K, Zhang Z, Kang S, Payabvash S, Sotiropoulos F: **Fluid dynamics simulations show that facial masks can suppress the spread of covid-19 in indoor environments**. *AIP Adv* 2020, **10**:125109.

76. Sahu RP, Sinha-Ray S, Yarin A, Pourdeyhimi B: **Drop impacts on electrospun nanofiber membranes**. *Soft Matter* 2012, **8**: 3957−3970.